iScience

Article

DPANN symbiont of *Haloferax volcanii* accelerates xylan degradation by the non-host haloarchaeon *Halorhabdus* sp.

Graphical abstract

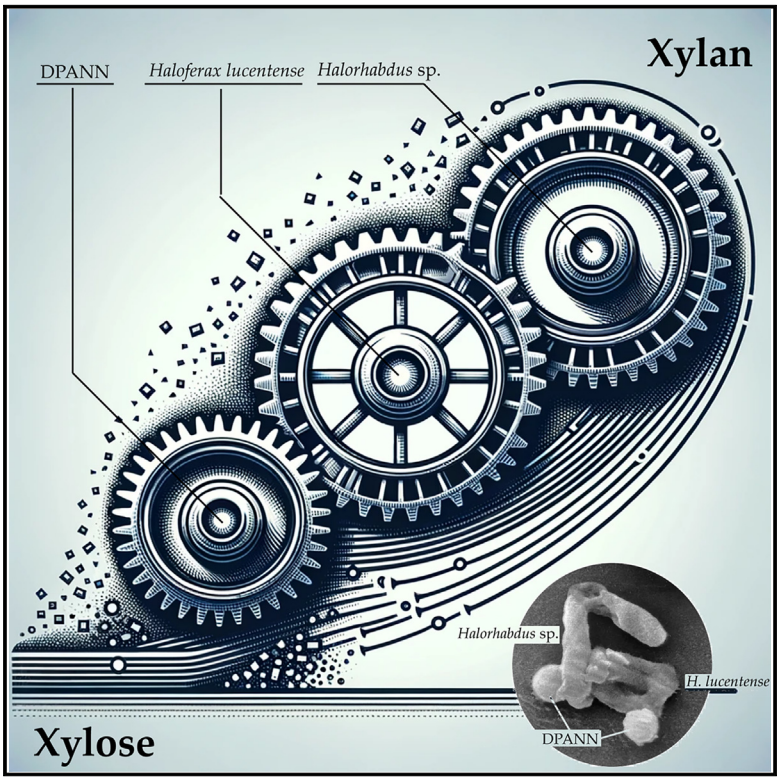

Highlights

- DPANN symbionts accelerate xylan degradation in the archaeal consortium
- DPANN symbiont aids glycolysis; others provide xylanases and essential synthesis
- Formation of heterocellular biofilms, interlinked by DPANN cells, was demonstrated
- DPANN impacts metabolism in all consortium members but requires its host to thrive

Authors

Oleg N. Reva, Violetta La Cono, Laura Marturano, ..., Laura Fernandez-Lopez, Mart Krupovic, Michail M. Yakimov

Correspondence

oleg.reva@up.ac.za (O.N.R.), mikhail.iakimov@cnr.it (M.M.Y.)

In brief

Biochemistry; Microbiology; Environmental Biotechnology

Reva et al., 2025, iScience *28*, 111749
February 21, 2025
https://doi.org/10.1016/j.isci.2025.111749

CellPress

iScience

CellPress
OPEN ACCESS

Article

DPANN symbiont of *Haloferax volcanii* accelerates xylan degradation by the non-host haloarchaeon *Halorhabdus* sp.

Oleg N. Reva,[1,*] Violetta La Cono,[2] Laura Marturano,[2] Francesca Crisafi,[2] Francesco Smedile,[2] Manasi Mudaliyar,[3,4] Debnath Ghosal,[3,4] Elena A. Selivanova,[5] Marina E. Ignatenko,[5] Manuel Ferrer,[6] Laura Fernandez-Lopez,[6] Mart Krupovic,[7] and Michail M. Yakimov[2,8,*]

[1]Department of Biochemistry, Genetics and Microbiology, Centre for Bioinformatics and Computational Biology, University of Pretoria, 0002 Pretoria, South Africa
[2]Extreme Microbiology, Biotechnology and Astrobiology Group, Institute of Polar Sciences, ISP-CNR, 98122 Messina, Italy
[3]Department of Biochemistry and Pharmacology, Bio21 Molecular Science and Biotechnology Institute, The University of Melbourne, Melbourne, 3052 VIC, Australia
[4]ARC Centre for Cryo-electron Microscopy of Membrane Proteins, Bio21 Molecular Science and Biotechnology Institute, University of Melbourne, Parkville, 3052 VIC, Australia
[5]Orenburg Federal Research Center, Institute for Cellular and Intracellular Symbiosis, Ural Branch of Russian Academy of Sciences, 460000 Orenburg, Russia
[6]Instituto de Catalisis y Petroleoquimica (ICP), CSIC, 28049 Madrid, Spain
[7]Institut Pasteur, Université Paris Cité, CNRS UMR6047, Archaeal Virology Unit, 75015 Paris, France
[8]Lead contact
*Correspondence: oleg.reva@up.ac.za (O.N.R.), mikhail.iakimov@cnr.it (M.M.Y.)
https://doi.org/10.1016/j.isci.2025.111749

SUMMARY

This study examines a natural consortium of halophilic archaea, comprising xylan-degrading *Halorhabdus* sp. SVX81, consortium cohabitant *Haloferax volcanii* SVX82 (formerly *H. lucentense* SVX82), and its DPANN ectosymbiont *Ca*. Nanohalococcus occultus SVXNc. Transcriptomics and targeted metabolomics demonstrated that the tripartite consortium outperformed individual and the *Halorhabdus* sp. SVX81 with *H. volcanii* SVX82 bipartite cultures in xylan degradation, exhibiting a division of labor: the DPANN symbiont processed glycolysis products, while other members performed xylan depolymerization and biosynthesis of essential compounds. Electron microscopy and cryo-electron tomography revealed the formation of heterocellular biofilms interlinked by DPANN cells. The findings demonstrated that DPANN symbionts can interact directly with other members of microbial communities, which are not their primary hosts, influencing their gene expression. However, DPANN proliferation requires their primary host presence. The study highlights the collective contribution of consortium members to xylan degradation and their potential for biotechnological applications in the management of hypersaline environments.

INTRODUCTION

Across all Earth's biomes, complex microbial consortia cycle organic and inorganic compounds, producing a significant portion of the planet's biomass.[1] The biotechnological uses of these consortia solve numerous human challenges and problems, from waste management to soil fertilization for agriculture. However, the question arises whether the individual microorganisms, even the most active ones, fully fulfill their potential when acting in isolation, outside of the natural microbial consortia. The advent of advanced RNA and DNA sequencing technologies has made it somewhat easier to model metabolic interactions within microbial consortia, including archaeal ones, known for their diverse metabolic pathways suited to extreme conditions.[2]

A case in point is consortia of halophilic archaea capable of degrading xylan in hypersaline environments around the globe. Xylans are the main structural heteropolysaccharides in plants, where they can constitute up to 30% of the dry weight of dicotyl plants, both herbaceous and hardwoods.[3] This polymer is second only to cellulose in abundance on Earth, and is thus a major reservoir of reduced carbon in the environment where roughly 10^{10} metric tons of xylans are turned over annually,[4] contributing to greenhouse gas emissions.[5] Thus, efficient breakdown of xylan-rich wastes helps to restore polluted and depleted environments.[6] However, near-saturating salt concentrations impede the growth of many xylan-degraders, highlighting the unique position of extreme halophiles in hypersaline habitats.[7–9]

Recent studies spotlight the DPANN superphylum, which comprises nanosized archaea previously overlooked as part of the "microbial dark matter",[10,11] living symbiotically or parasitically on other archaea or bacteria. Due to their reduced genomes and depleted metabolic pathways, cultivation of DPANN archaea

Table 1. Four experimental arrangements used in this study to elucidate intrinsic interactions between the archaeal consortium members using transcriptomics

Experiments	Carbone source	SRA accession	Number of reads
Axenic culture			
I. *H. volcanii* SVX82	D-Xylose	SRX22141247	23,511,982
		SRX22141248	20,164,144
Bipartite cultures			
II. *H. volcanii* SVX82 + *Ca*. N. occultus SVXNc	D-Xylose	SRX22141249	25,347,949
		SRX22141236	24,042,256
III. *Halorhabdus* sp. SVX81 + *H. volcanii* SVX82	Beech wood Xylan	SRX22141237	21,807,457
		SRX22141238	18,522,458
Tripartite culture			
IV. *Halorhabdus* sp. SVX81 + *H. volcanii* SVX82 + *Ca*. N. occultus SVXNc	Beech wood Xylan	SRX22141239	19,204,142
		SRX22141240	21,650,662
		SRX22141241	22,735,729

outside of host environments thus far proved impossible.[12–14] The functional role of DPANN archaea in the biosphere remains largely enigmatic.[15,16] Are they friends or foes in natural environments, and do they play an important and cohesive role in microbial consortia that decompose waste? Here, we take a closer look at a three-membered, extremely halophilic natural consortium consisting of the xylan-degrading *Halorhabdus* sp. SVX81, its associate *Haloferax lucentense* SVX82, and the DPANN archaeon *Candidatus* Nanohalococcus occultus SVXNc, an ectosymbiont of *H. lucentense*.[12,13] *H. lucentense* has been recently reclassified as *Haloferax volcanii*[17]; therefore, this taxonomic name is used throughout this paper for the strain SVX82.

Through transcriptomics, targeted metabolomics, scanning electron microscopy (SEM), and cryo-electron tomography (cryo-ET), we explored the intrinsic interactions among members of this natural tripartite consortium, aiming to uncover its biotechnological potential for xylan degradation and to advance research on complex microbial communities in extreme environments.

RESULTS

Xylan degradation and quantitative analysis of xylooligosaccharides

Three xylan-degrading experimental consortia of archaea, along with an *H. volcanii* SVX82 axenic culture, were used in this study (Table 1). Xylan degradation activities of the consortia were compared to that of the axenic *Halorabdus* sp. SVX81 culture. After 240 h of cultivation, biomass growth significantly slowed in all three cultures used in this experiment: axenic *Halorhabdus* sp. SVX81 (*Hr*), the bipartite culture with *H. volcanii* SVX82 (*Hr+Hv*), and the tripartite culture with *Ca*. N. occultus SVXNc (*Hr+Hv+No*), leaving residual xylan amounts (Table 2). The reduced growth rate could be due the depletion of essential nutrient, such as vitamins, and the accumulation of toxic byproducts resulting from the static cultivation conditions of this experiment. Xylan concentration in the flasks with cultures in triplicates was measured at the beginning of the experiment (before inoculation) and at three time points: 72, 120, and 240 h of cultivation. The dynamics of xylan consumption and biomass increase are shown in Figure 1. The analysis of the presence of X_1–X_4 xylooligosaccharides in the supernatants is presented in Table 2.

The yield of xylooligosaccharides, detected in the *Hr* axenic culture after 120 h of cultivation showed comparable concentrations of xylose, xylobiose, xylotriose, and xylotetraose (26%, 20%, 32%, and 22%, respectively). The presence of *Haloferax* in the *Hr+Hv* bipartite culture caused a significant depletion of xylooligosaccharides, with their concentrations falling below the detection limit at 120 and 240 h of cultivation. Xylose was detected only midway through the experiment at 120 h of cultivation. Although *H. volcanii* SVX82 cannot degrade xylan due to the lack of xylanases, it can consume xylose as a monomeric product of xylan hydrolysis, which is the only product accessible to this organism.[13] We hypothesize that the depletion of monosaccharides in the *Hr+Hv* bipartite culture medium may create energy constraints for *Halorhabdus* sp. SVX81, resulting in a slightly delayed xylan degradation by the *Hr+Hv* consortium compared to the axenic *Hr* culture (Figure 1). However, this delay constantly recorded at all three time point, was statistically insignificant, with *p* values ranging from 0.27 at 240 h to 0.68 at 72 h.

An intriguing discovery was that the presence of the *H. volcanii*'s ectosymbiont, *Ca*. N. occultus SVXNc, affected both the kinetics of xylan degradation by the consortium and the amount of xylose and xylooligosaccharides in the tripartite culture medium (Figure 1 and Table 2). Specifically, after 120 h of cultivation, the tripartite culture was enriched in xylose compared to other consortia, comprising 94.5% of the total X1-X4 xylooligosaccharides detected. The xylose concentration in the medium increased to 179 mg L^{-1}, indicating a significant increase in xylose production beyond the consortium's consumption capacity. The difference in xylan consumption by the *Hr+Hv+No* consortium was statistically significant compared to the *Hr* axenic culture (*p* value 0.035) and showed a notable trend compared to the *Hr+Hv* consortium (*p* value 0.091) at the 120 h time point of cultivation. Xylan consumption slowed in all consortia and became indistinguishable after 240 h of cultivation due to methodological constraints of the static growth experiment. The *Hr+Hv+No* culture outperforms other cultures in terms of biomass accumulation at all three time points; however, this difference was statistically insignificant (Figure 1).

A possible shift in the metabolism of both haloarchaea in response to the presence of a nanohaloarchaeal ectosymbiont was further analyzed using comparative transcriptomics.

Differential gene expression in *H. volcanii* SVX82

Gene expression patterns of *H. volcanii* SVX82 were analyzed under four conditions described in Table 1. The full list of genes and the average reads per kilo base per million mapped reads (RPKM) values for each experimental group are shown in Table S1. To determine whether *H. volcanii* SVX82 exhibits different gene expression patterns in different consortia, principal-component analysis (PCA) was used to plot all experiments and estimate 95% confidence ellipses around dots representing experimental repetitions of the same consortia (Figure S1). The axenic culture (*Hv*) and the *Hv+No* bipartite consortium

Table 2. Kinetics of xylan degradation and biomass accumulation by axenic culture of *Halorhabdus* sp. SVX81, as well the *Hr+Hv* bipartite and the tripartite cultures, containing this xylan-decomposing haloarchaeon

Experiment	Cultivation, h	Biomass, mg L^{-1}	Xylan remaining, mg L^{-1}	Xylooligosaccharides detected, mg L^{-1}			
				X_1	X_2	X_3	X_4
Abiotic control	72	NA	1,840 ± 80[a]	0[b]	0	0	0
	240	NA	1,800 ± 50	0	0	0	0
Axenic culture							
Halorhabdus sp. SVX81	72	183 ± 45	1,667 ± 115	27	20	80	48
	120	197 ± 29	1,033 ± 58	49	37.5	60	42
	240	383 ± 161	667 ± 58	53	80.5	86	0
Hr+Hv bipartite culture							
Halorhabdus sp. SVX81 + *H. volcanii* SVX82	72	167 ± 76	1,550 ± 212	0	0	30	26
	120	250 ± 71	1,133 ± 208	56	0	0	0
	240	433 ± 58	767 ± 115	0	0	0	0
Tripartite culture							
Halorhabdus sp. SVX81 + *H. volcanii* SVX 82 + *Ca*. N. occultus SVXNc	72	183 ± 29	1,400 ± 173	13	123	105	14
	120	267 ± 58	800 ± 100	179	4.5	6	0
	240	483 ± 29	583 ± 115	14	0	0	0

X_1, Xylose; X_2, Xylobiose; X_3, Xylotriose; X_4, Xylotetraose; NA, not applicable.
[a]Mean value ±standard deviation.
[b]0, the concentration of the compound was below the sensitivity of the method used.

(experimental settings I and II) exhibited similar, statistically indistinguishable patterns of gene expression, whereas the gene expression patterns in the bipartite *Hv+Hr* and the tripartite consortia (III and IV) significantly differed from each other and from those exhibited by consortia I and II. The statistical significance of differential gene expression was also confirmed by a PERMANOVA test, with a p value of 0.01. It should be noted that despite the general similarity in all-gene expression patterns between consortia I and II, there were genes showing statistically significant differences in their expression (see in the following text.).

Further analysis was conducted to identify metabolic pathways-associated genes that were differentially expressed in different consortia. Genes were linked to metabolic pathways using Pathway Tools v26.0, and their expression was compared to that in the *H. volcanii* SVX82 axenic culture (experimental group I). This comparison allowed for the selection of 38 core genes representing different metabolic pathways, which were differentially expressed with a fold change of two or greater and a p value of ≤ 0.05 in at least one pair of compared consortia. Average RPKM values of these genes across the four consortia are shown in Table S2. These values were used for PCA plotting, as shown in Figure 2, where loadings of individual pathway-associated genes are represented as vectors pointing toward the plotted locations of the consortia (nodes labeled from I to IV) in which these genes exhibited the highest expression.

PCA revealed distinct metabolic changes in each experimental group. The presence of *Ca*. N. occultus SVXNc in the *Hv+No* bipartite culture (experimental group II) caused only minor changes in expression of genes involved in metabolic pathways of *H. volcanii* SVX82 compared to its axenic culture (M-plot of gene regulation is shown in Figure S2A). However, this strain grown in a consortium with *Halorhabdus* sp. SVX81 (experimental group III) exhibited significant changes in gene regulation (as shown in Figure S2B). As shown in the PCA plot in Figure 2, there is likely an activation of the expression of SVX82 genes associated with gluconeogenesis and the Entner-Doudoroff pathway, along with the transcriptional activation of sugar transport systems, several anabolic pathways, nucleotide and amino acid biosynthesis. These changes are most likely due to apparent competition between the haloarchaea *Hr* and *Hv* for the uptake of newly formed xylose, which, as shown in Table 2, is present in the culture medium in minor quantities (less than 60 mg L^{-1}), compared to experimental groups I and II, where this monosaccharide is readily available to *H. volcanii* SVX82 (2,000 mg L^{-1}).

Interestingly, the presence of *Ca*. N. occultus SVXNc in the tripartite consortium considerably altered the metabolism of *H. volcanii* SVX82, markedly enhancing the synthesis of secondary metabolites and adjusting metabolic pathways compared to its axenic culture and the *Hv+No* bipartite consortium (experimental groups I and II grown on D-xylose). The strong activation of pyruvate decarboxylase and the glyoxylate shunt suggests that pyruvate and acetate became not only the primary sources of energy but also the main source of carbon for biosynthetic reactions. Increased expression of genes encoding tRNA charging proteins suggests that protein biosynthesis by *H. volcanii* SVX82 was activated in the tripartite culture. For several genes expressed in axenic *H. volcanii* SVX82, transcripts were not detected in the tripartite culture (Table S3), likely due to cooperation among consortium members. Such genes include, for example, Entner-Doudoroff pathway aldolase *eda* and three paralogous copies of 2-dehydro-3-deoxygluconokinase *kdgK*; 3-dehydroquinate dehydratase *aroD* involved in chorismate biosynthesis in

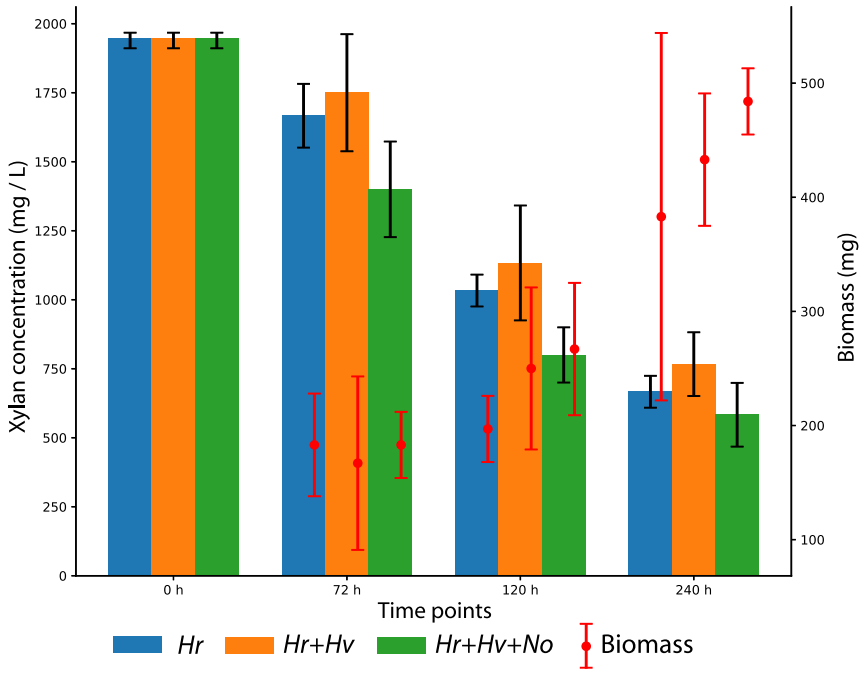

Figure 1. Xylan concentrations and biomass accumulation over time in three consortia

Hr – axenic *Halorhabdus* sp. SVX81; *Hr+Hv* – *Halorhabdus* sp. SVX81 + *H. volcanii* SVX82; *Hr+Hv+No* – *Halorhabdus* sp. SVX81 + *H. volcanii* SVX 82 + *Ca*. N. occultus SVXNc. Data are represented as mean +/− standard deviation.

archaea; cobalt-precorrin-6B (C15)-methyltransferase *cbiT* and adenosylcobinamide amidohydrolase *cbiZ* involved in Cob(II)yrinate a,c-diamide biosynthesis and adenosylcobinamide-GDP salvage; multiple chemotaxis and archaellum biogenesis genes; as well as a number of transcriptional regulators. This alteration in metabolism highlights the complex trophic interactions within the consortium, which are influenced by the presence of the symbiont and varying growth conditions.

Differential gene expression in xylan-degrading *Halorhabdus* sp. SVX81

Halorhabdus sp. SVX81 is the only archaeon in the tripartite consortium capable of hydrolyzing xylan to xylooligosaccharides and xylose, providing its community partners with essential energy and carbon sources.[14] It grows independently on xylan, but in the tripartite consortium, *Halorhabdus* sp. SVX81 shows a statistically significant increase in xylan degradation efficiency compared to both its axenic culture and the *Hr+Hv* bipartite culture (Figure 1 and Table 2). In a previous study,[13] we investigated the association of *Ca*. N. occultus SVXNc with *H. volcanii* SVX82 in the *Hv+No* bipartite culture grown on D-xylose, corresponding to experimental group II but did not assess the ectosymbiont's colonization specificity in the tripartite consortium. The enhanced degradation observed under these conditions may have been due to either the direct physical association or indirect influence of *Ca*. N. occultus SVXNc on the metabolism of *Halorhabdus* sp. SVX81, despite the previously reported inability of the ectosymbiont to stably grow on *Halorhabdus* sp. SVX81 when these two organisms were attempted to be cultured together in the absence of *H. volcanii* SVX82.[13]

In the tripartite culture with *Ca*. N. occultus SVXNc, grown on xylan as the sole source of energy and carbon, *Halorhabdus* sp. SVX81 exhibited significant changes in gene expression (M-plot in Figure S2C). A detailed analysis of genes homologous between *Halorhabdus* sp. SVX81 and *H. volcanii* SVX82 revealed 1,572 shared genes, with 1,174 protein-coding genes being up- and downregulated under the studied conditions (Table S4). The analysis of the expression patterns of genes homologous between *Halorhabdus* sp. SVX81 and *H. volcanii* SVX82, under the influence of *Ca*. N. occultus SVXNc, revealed a statistically significant degree of metabolic co-regulation between them, indicated by a Pearson correlation of 0.262 and supported by a two-tailed p value of $1.8e^{-8}$ (Figure 3). The correlation coefficient increased to 0.317 when all genes encoding unknown and hypothetical proteins were filtered out. This co-regulation includes 27 transcriptional regulators and multiple genes for ribosomal proteins displaying synchronous up- and downregulation. This result highlights adaptive shifts in protein synthesis in the tripartite consortium. Notably, key pathways such as glycolysis/gluconeogenesis were broadly downregulated, while enzymes involved in the tricarboxylic acid cycle (TCA) cycle and acetate-CoA metabolism were upregulated, showcasing a metabolic pivot to accommodate communal propagation. The observed gene co-regulation suggests a concerted metabolic response of these two haloarchaeal consortium members to the introduction of *Ca*. N. occultus SVXNc, which is difficult to explain solely through the indirect action of the symbiont on *Halorhabdus* cells. Thus, based on the transcriptome data, we propose that *Ca*. N. occultus SVXNc can interact with *Halorhabdus* sp. SVX81 when its host, *H. volcanii* SVX82, is present in the community. However, given that the symbiont does not grow on *Halorhabdus* cells in binary culture, for reasons that remain to be understood, we suggest that colonization of the xylan degrader by the ectosymbiont in the tripartite consortium, even if transient, nevertheless occurs and tends to rewire the metabolism of *Halorhabdus*, shifting it toward increased production of xylose—the only xylan hydrolysis product accessible for the true host of the ectosymbiont, *H. volcanii* SVX82.

Differential gene expression in the symbiotic archaeon *Ca*. N. occultus SVXNc

The cultivation of the DPANN archaeon *Ca*. N. occultus SVXNc in the tripartite xylan-degrading consortium notably affected its gene expression, in contrast to its growth on the xylose-utilizing host in binary culture (M-plot is in Figure S2D; the full list of

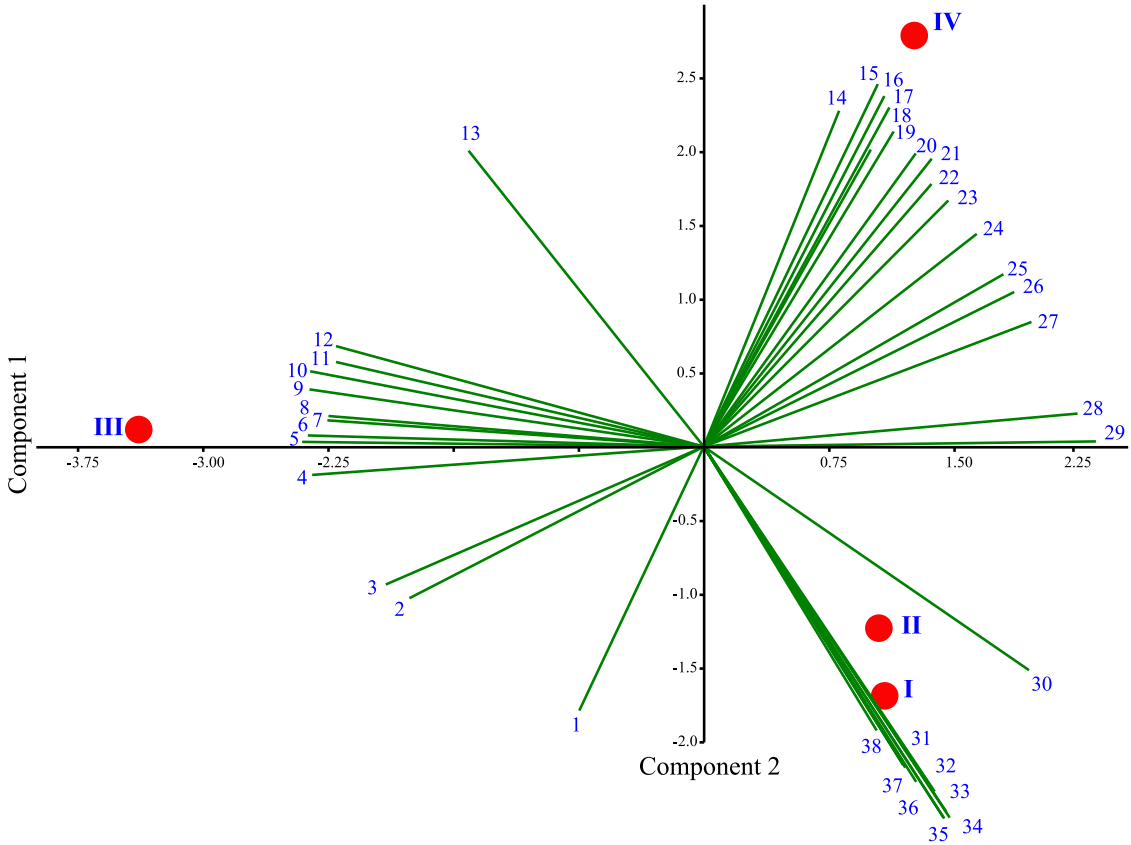

1. Mulitocopper oxidase
2. Nitric oxide reductase
3. L-serine biosynthesis I
4. Factor 420 biosynthesis I (archaea)
5. NADPH:quinone reductase
6. Gluconeogenesis I
7. Inorganic pyrophosphatase
8. Archaeal/vacuolar-type H+-ATPase
9. Entner-Doudoroff pathway III, gluconeogenesis I
10. Archaellum pili biosynthesis
11. Translation elongation factor 1 alpha subunit
12. Peroxiredoxin
13. PRPP biosynthesis
14. Molybdenum cofactor biosynthesis
15. ABC-type dipeptide/oligopeptide/nickel transporter
16. ABC-type Mn/Zn transporter
17. Ammonium transporter
18. [2Fe-2S] iron-sulfur cluster biosynthesis
19. Mevalonate pathway II in haloarchaea
20. Tetrapyrrole biosynthesis I (from glutamate)
21. Glyoxylate shunt
22. Shikimate/chorismate/3-dehydroquinate synthesis in archaea
23. Phosphoribosyl 1,2-cyclic phosphate phosphodiesterase
24. tRNcharging
25. Nicotinamide biosynthesis
26. Pyruvate decarboxylation to acetyl CoI
27. Ribosome maturation
28. tRNA(Ile)-lysidine synthase
29. Flavin biosynthesis II (archaea)
30. Ferrodoxin oxidoreductase
31. ABC-type branched-chain amino acid transporter
32. Alpha-L-Glutamate lyase
33. Pyrimidine nucleobases salvage and de novo biosynthesis
34. Mesaconyl-CoA hydratase
35. Cob(II)yrinate a,c-diamide biosynthesis I
36. Na+/H+-dicarboxylate symporter
37. 4-Hydroxythreonine-4-phosphate dehydrogenase
38. Galactitol PTS system

Figure 2. The principal-component analysis (PCA) biplot shows the eigenvectors of different metabolic pathways, which exhibit dissimilar gene expression in the tested archaeal consortia, and distribution of the gene expression patterns of *H. volcanii* SVX82 in different consortia

(I) axenic monoculture on xylose; (II) bipartite co-culture with *Ca*. N. occultus SVXNc on xylose; (III) *Hr+Hv* bipartite culture; and (IV) tripartite co-culture on xylan. The gene expression patterns are depicted by thick red dots, plotted according to their eigenvalues of the first two principal components. The eigenvectors of the metabolic pathways are represented as green lines, directed toward the gene expression plots where they exhibit the highest expression or in the opposite direction from the patterns where they were most inhibited. The lengths of the vector lines correspond to the relative loadings of the eigenvectors.

regulated genes is in Table S5). In particular, the archaeal/vacuolar-type H-ATPase and glucose-6-phosphate isomerase genes were significantly upregulated in the ectosymbiont, although they were suppressed in *H. volcanii* SVX82 and *Halorhabdus* sp. SVX81 within the same consortium. This activation suggests active acetyl-CoA and/or succinyl-CoA synthesis, which could subsequently be transported to host cells, given that *Ca*. N. occultus SVXNc lacks a functional TCA cycle.[14] The activation of two glycosyltransferase genes may facilitate the processing of host-derived carbohydrates. The majority of glycolytic enzymes

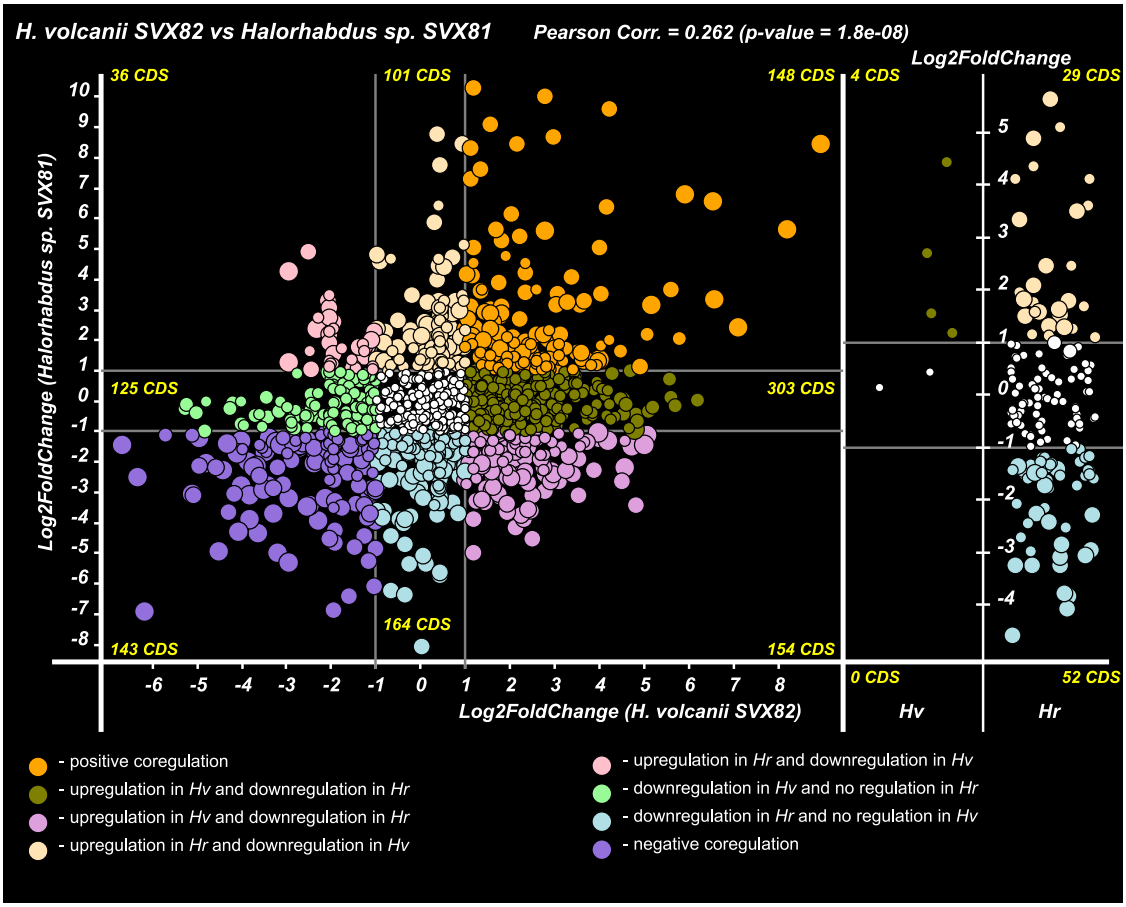

Figure 3. The plot of co-regulation of homologous genes in *Halorhabdus* sp. SVX81 (*Hr*) and *H. volcanii* SVX82 (*Hv*)

Each colored dot represents a pair of homologous genes from the two genomes. These pairs are plotted based on their Log_2(fold_change) values, comparing the *Hr+Hv* bipartite and tripartite consortia on xylan, respectively for *Halorhabdus* sp. SVX81 (x axis) and *H. volcanii* SVX82 (y axis). Co- and counter-regulated gene pairs are differentiated by dots of various colors, as detailed in the figure legend. The dots on the two right panels represent pairs of homologous genes that were expressed and regulated exclusively in either *H. volcanii* (panel titled "*Hv*") or *Halorhabdus* sp. SVX81 (panel titled "*Hr*"). The distribution of the dots in these panels corresponds to their Log_2(fold_change) values. The estimated Pearson correlation and the two-tailed *p* value are also displayed on the plot.

remained consistently expressed. The upregulation of genes responsible for biogenesis of the archaellum and type IV pili implies a potential role for the symbiont in formation of biofilm-like networks to interact with the host cells and, possibly, with other consortium members.

Significant downregulation of 15 ribosomal protein genes mirrors similar adjustments in *H. volcanii* SVX82 and *Halorhabdus* sp. SVX81, aimed at optimizing ribosome function under new conditions. Moreover, the downregulation of several RNA polymerase subunits might adjust gene transcription, alongside numerous other genes that are differentially expressed.[18] The genes differentially expressed in this experiment are listed in Table S3. However, the biological implications of these changes remain challenging to fully interpret due to a limited understanding of the biology and metabolism of nano-sized DPANN archaea. Based on these data, it can be assumed that the suppression of many genes in *Ca*. N. occultus SVXNc, detected in the tripartite consortium compared to the binary culture, can likely be explained by the increased influx of a much broader spectrum of metabolites, cofactors, and biosynthesis precursors between the ectosymbiont and host cells, including *Halorhabdus* sp., due to its aforementioned, even if transient, association with *Ca*. N. occultus SVXNc.

Intracellular interactions between consortium members

The observed co-regulation of genes between *Halorhabdus* sp. SVX81 and *H. volcanii* SVX82, influenced by the presence of *Ca*. N. occultus SVXNc, underscores the complexity of microbial consortia and the extent to which symbionts can influence all members of the consortium, including those that are not their primary hosts. This transcriptome-based inference was confirmed by the scanning electron microscopy (SEM) analysis of the tripartite consortium, which showed that *Ca*. N. occultus SVXNc, the ectosymbiont of *H. volcanii*, indeed interacts with both: its primary host (Figure 4A) and *Halorhabdus* cells (Figure 4B). Dividing ectosymbiont cells were observed on the surface of both haloarchaeal members of the tripartite consortium. Notably, at the early stages of cultivation (72 h), the proportion of *Halorhabdus* sp. SVX81 cells associated with nanohaloarchaea was already

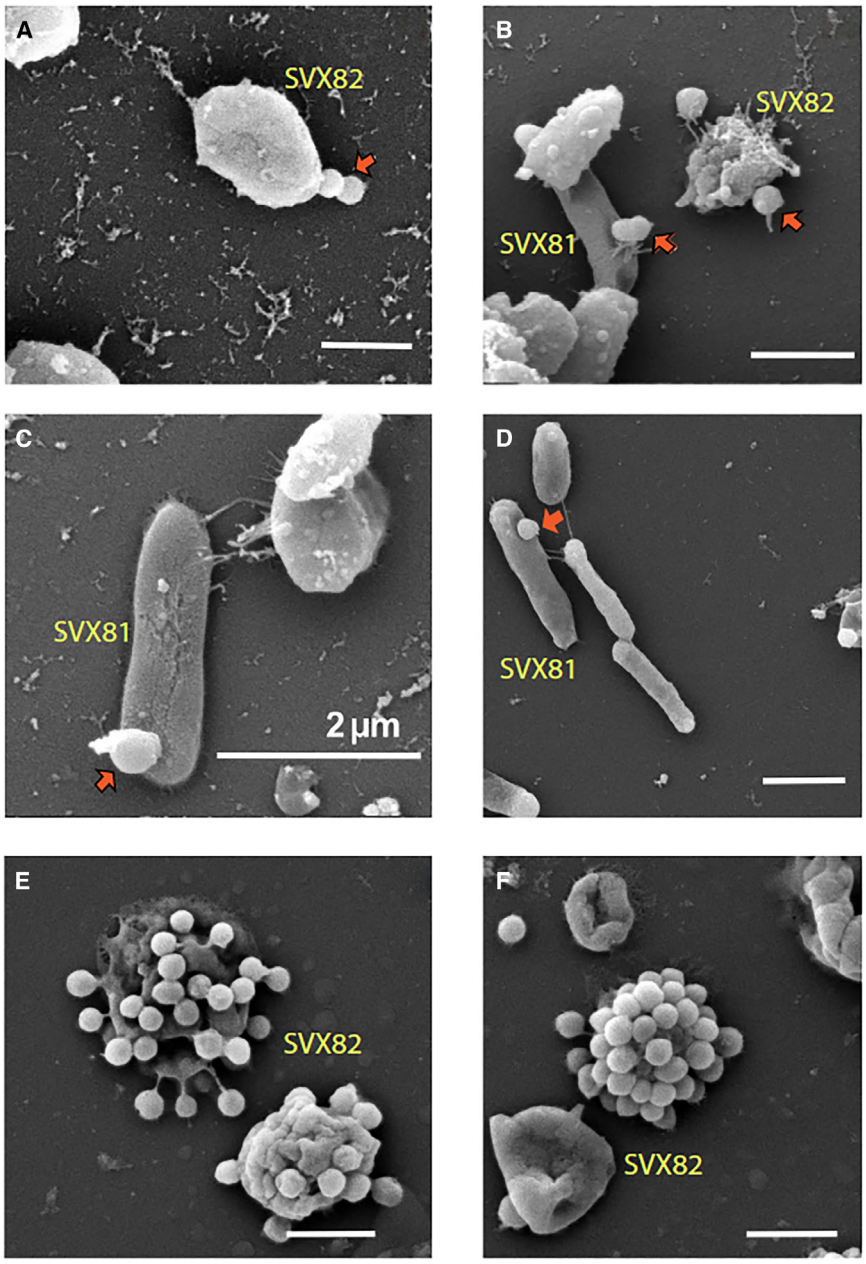

Figure 4. Scanning electron microscopy (SEM) images of the colonization of cells of archaeal consortium members by the DPANN ectosymbiont *Ca*. N. occultus SVXNc

All scale bars in the figure correspond to 2 µm.

(A) Colonization of the primary host, *H. volcanii* SVX82 visualized at 72 h of cultivation; (B) Cells of the ectosymbiont on the cells of two species, *H. volcanii* SVX82 and *Halorhabdus* sp. An arrow indicates a *Ca*. N. occultus cell that has begun division on the surface of a *Halorhabdus* cell; (C and D) Colonization of cells of the xylan-degrading consortium cohabitant *Halorhabdus* sp. SVX81 by the ectosymbiont visualized at 120 h of cultivation; (E and F) Hypercolonization of cells of *H. volcanii* SVX82 by the DPANN ectosymbiont visualized after one month of cultivation. In all SEM photos, cells of the DPANN ectosymbiont *Ca*. N. occultus SVXNc are indicated by arrows. Cells of *H. volcanii* SVX82 and *Halorhabdus* sp. were distinguished based on cell morphology, as explained in the STAR Methods.

7.20 ± 1.04% (n = 677). However, this fraction was significantly lower compared to that of ectosymbiont SVXNc cells attached to *H. volcanii* SVX82 (13.05 ± 0.47%; n = 359). This disparity is partly due to the fact that while *Ca*. N. occultus SVXNc formed an association with *Halorhabdus* sp. SVX81 with a median multiplicity of only one cell per host cell, the median multiplicity of ectosymbiont cells attached to one *H. volcanii* SVX82 cell was much higher: two to four cells per host cell. At a later stage of cultivation (120 h), the proportion of *Halorhabdus* cells showing association with *Ca*. N. occultus SVXNc increased to 14.18 ± 1.86% (n = 231) (Figure 4C). The median multiplicity of nanohaloarchaeal cells attached to *Halorhabdus* did not change with the time of cultivation, while the average number of cells attached to *H. volcanii* SVX82 increased significantly, accounting for more than 95% of all detected ectosymbiont cells.

Inhabitants of the halophilic xylan-degrading consortium formed a complex heterocellular biofilm matrix, as shown in extended data Figure S2A. Moreover, a pattern of tight attachment of one nanohaloarchaeal cell to both *Halorhabdus* sp. SVX81 and *H. volcanii* SVX82 cells was often observed (Figures S2B–S2E). Further studies should clarify whether an exchange of metabolites between *H. volcanii* and *Halorhabdus* cells through the bridging DPANN symbionts is possible. Numerous free symbiotic cells unattached to host cells were also observed in the tripartite consortium during the SEM observations. In addition to the previously described pore formation, SEM analysis revealed another mode of interaction between the symbiotic DPANN cells and host cells. Namely, thin, long stalks resembling pilus-like structures or intracellular channels were observed to connect either the ectosymbiont and the host cells or the ectosymbiont cells themselves (Figures S2F–S2J).

Additionally, we set out to test whether the ectosymbiont remains attached to the *Halorhabdus* cells under conditions when all the digestible substrate has already been consumed and the consortium is in deep starvation mode. In a month-old tripartite culture, no infected *Halorhabdus* cells were detected, while the median multiplicity of nanohaloarchaeal cells attached to *H. volcanii* increased significantly, with more than 20–25 cells of the ectosymbiont found attached to a single *H. volcanii* host cell (Figures 4E and 4F).

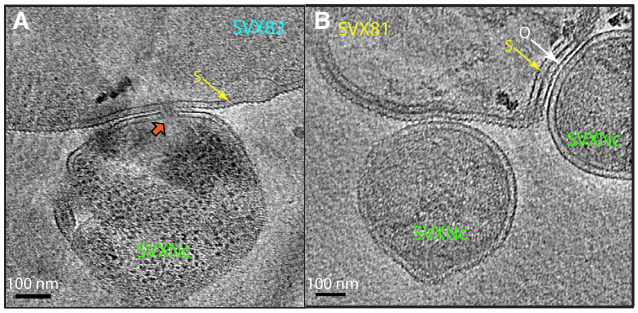

Figure 5. Cryo-electron tomography images of the interaction between the DPANN symbiont and its host, *H. volcanii* SVX82, as well as the non-host member of the archaeal consortium, *Halorabdus* sp. SVX81

Features, morphologies and interaction events observed between (A) *H. volcanii* SVX82 and *Ca*. N. occultus SVXNc, and (B) *Halorhabdus* sp. SVX81 and *Ca*. N. occultus SVXNc. Scale bars represent 100 nm. Pore formation between the cells of *H. volcanii* and *Ca*. N. occultus is indicated by a thick red arrow. Surface layers (S-layers) in both organisms and an outer layer (O-layer) in the double-layered structure of the cell wall of *Halorhabdus* sp. SVX81 are indicated by yellow and white thin titled arrows, respectively.

Further insight into the physical interactions between the *Ca*. N. occultus SVXNc ectosymbiont and its natural and transient hosts, *H. volcanii* and *Halorhabdus*, was obtained using cryo-ET that revealed potential mechanisms for metabolite exchange through extracellular structures. Recent studies have reported that DPANN archaea interact with their host and exchange metabolites through pores and cytoplasmic tunnels penetrating cellular membranes.[19,20] These structures were hypothesized to facilitate the exchange of not only metabolites but also proteins, such as methyltransferases.[21] The interaction between the symbiont and the *H. volcanii* host involves the formation of a cytoplasmic bridge that traverses the S-layers of both cells, as indicated by a red thick arrow in Figure 5A. Cryo-ET confirmed the binding of *Ca*. N. occultus cells to *Halorhabdus* (Figure 5B); however, the physical mechanism of this interaction likely differs. No pore formation was observed between the cells, but the visible local depression of the *Halorhabdus*'s cell wall at the site of contact with the *Ca*. N. occultus cells suggests a rather tight interaction between the organisms. The difference in physical interaction mechanisms between the cells of the symbiont and the cells of *H. volcanii* and *Halorhabdus* is likely associated with the obvious differences in the cell wall structures of these two species of halophilic archaea. *H. volcanii* has a typical archaeal surface layer (S-layer) surrounding a single lipid membrane,[22] whereas, for *Halorhabdus* sp. SVX81, cryo-ET analysis revealed a complex and unusual double-layered cell wall structure with an additional outer layer (Figure 5B).

DISCUSSION

Intrinsic relationships between cohabiters in an environment can be understood through analyzing gene co-expression and transcriptional regulation, reflecting nutrient availability, environmental stresses, and consortium composition.[23,24] Here, we examined a natural consortium of three extremophilic archaeal organisms: *Halorhabdus* sp. SVX81, capable of hydrolyzing xylan; *H. volcanii* SVX82, a free-living archaeon that grows on xylose formed during the hydrolysis of xylan by *Halorhabdus* sp. SVX81; and *Ca*. N. occultus SVXNc, a nano-sized ectosymbiont of *H. volcanii* SVX82 from the DPANN superphylum, characterized by a theoretically predicted minimal cell size[25] and a highly reduced genome.[14] The dependence of DPANN archaea on their hosts for key biosynthetic precursors, such as amino acids, nucleotides, fatty acids, and cofactors, due to their compromised anabolic pathways, is evident. For example, the activation of genes involved in amino acid synthesis is observed in *H. volcanii* SVX82 in the presence of the ectosymbiont. Despite having highly restricted metabolic pathways, *Ca*. N. occultus SVXNc maintains a functional glycolysis pathway,[14] suggesting that it contributes its glycolytic capacity to supplement its host's biosynthetic potential.

Colonization of *H. volcanii* SVX82 by *Ca*. N. occultus SVXNc alters the host's metabolism, notably downregulating its glycolytic pathways. This interaction suggests a complex exchange of metabolites, with *Ca*. N. occultus SVXNc potentially providing glycolysis products to its host. Interestingly, the suppression of glycolysis, accompanied by sustained phosphorylation of carbohydrates by glucokinase in *H. volcanii* SVX82 colonized by the ectosymbiont, leads to a 50-fold increase in the concentration of phosphorylated glucose in its cytoplasm.[13] This suggests a tight metabolic relationship between the symbiont and its host.

This study demonstrates that microbial consortia, such as the one described herein, can outperform pure cultures in biotechnological applications, like xylan degradation. While *Halorhabdus* sp. SVX81 alone degrades xylan, *H. volcanii* SVX82 can contribute only to oligosaccharide degradation but utilizes xylose produced by *Halorhabdus* sp. SVX81, also supporting its symbiont *Ca*. N. occultus SVXNc (Figure 1 and Table 2). Contrary to the initial belief that *Halorhabdus* sp. SVX81 is the sole supporter of the consortium, a complex network of metabolic exchanges was uncovered, whereby the combined consortium's biodegradation capability exceeds the individual capacities with the demonstrated statistical significance at the 120 h time point of cultivation (Figure 1). This necessitates numerous metabolic adjustments among all members, challenging the simplistic view of one consortium provider and multiple consumers.

The DPANN symbiont may function as an "external mitochondrion," responsible for glycolysis, energy production, and possibly the maintenance of the transmembrane proton potential, shared with the host cells through the activation of the archaeal/vacuolar-type H^+ ATPase. However, these hypotheses, derived from gene regulation analysis, require experimental confirmation in future studies. *Halorhabdus* sp. SVX81 and *H. volcanii* SVX82 use metabolites from *Ca*. N. occultus SVXNc for synthesis of essential biomolecules and, in return, may supply carbohydrates. Thus, the three organisms exist in a mutualistic relationship facilitated by close cellular interactions, as evidenced by SEM (Figure 4) and cryo-ET (Figure 5). The interactions between the ectosymbiont *Ca*. N. occultus SVXNc and its host *H. volcanii* SVX82 deduced from the transcriptomics study (Tables S5 and S6) are summarized in Figure 6.

Gene co-regulation between *Halorhabdus* sp. SVX81 and *H. volcanii* SVX82 indicates direct symbiotic interaction, which

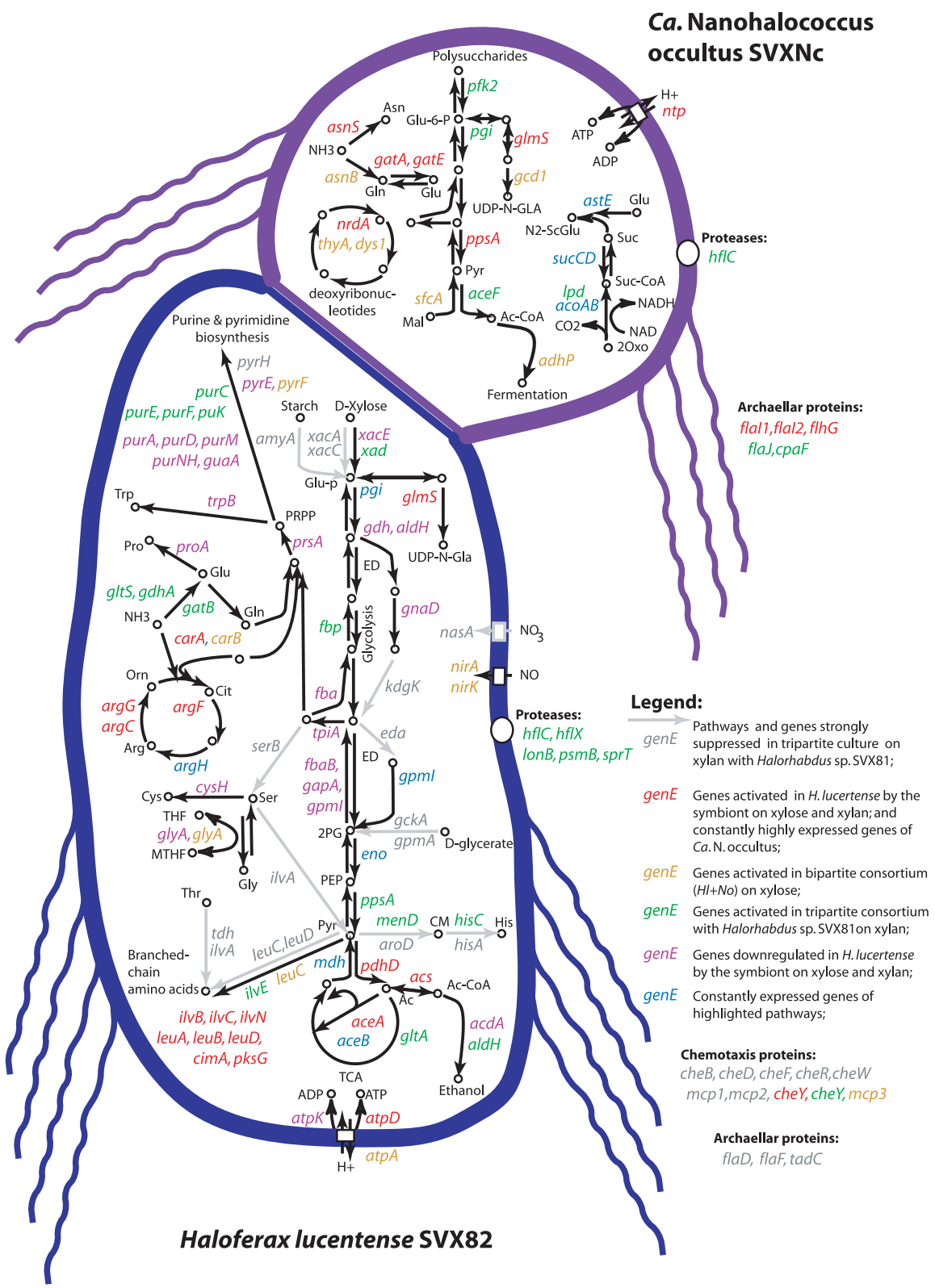

(legend on next page)

is a novel discovery contrasting our previous findings that *Ca*. N. occultus SVXNc cannot establish a stable binary co-culture with *Halorhabdus* sp. SVX81.[13] The hypothesis of the direct interaction between *Halorhabdus* cells and the DPANN ectosymbiont was confirmed by SEM (Figure 4) and cryo-ET (Figure 5). To our knowledge, this is the first observation of DPANN archaea being capable of simultaneous attachment to different hosts belonging to distinct orders.

One possible reason for the inability of *Ca*. N. occultus SVXNc to maintain permanent growth on *Halorhabdus* cells in a binary culture is the complex structure of the cell-wall of this archaeon, which differs from the single S-layer surrounding *H. volcanii*'s cells.[22] The double-layered cell wall revealed for *Halorhabdus* sp. SVX81 by cryo-ET (Figure 5), is uncommon for archaea, with only a few species having similar structures, such as *Ignicoccus hospitalis*, *Methanomassiliicoccus luminyensis*, and several members of the archaeal Richmond Mine acidophilic nanoorganisms (ARMAN group).[26] However, all these archaea are phylogenetically distant from *Halorhabdus*. To the best of our knowledge, the structure of the cell wall of *Halorhabdus* has not been studied until now.

Another factor influencing interactions between the symbiont and *Halorhabdus* cells can be the metabolic deficiencies of *Halorhabdus*, which lacks functional gluconeogenesis and has an incomplete TCA cycle due to the absence of several important genes, such as 2-oxoglutarate dehydrogenase that converts oxoglutarate to succinyl-CoA, fueling the anabolic part of the TCA and gluconeogenesis.[27] Additionally, *Halorhabdus* sp. lacks the glyoxylate shunt, necessary for using acetate for cell growth.[28] Regardless of the reason, the inability of the DPANN symbiont to stably thrive on *Halorhabdus* underscores the essential role of *H. volcanii* in maintaining the integrity of the tripartite archaeal consortium. This interdependency leads to an optimized consortium for degrading xylan waste more effectively.

A striking discovery was that the increased xylan degradation activity by the tripartite consortium exceeds the consortium's need for xylose, resulting in the accumulation of the sugar in the medium (Table 2). This sugar accumulation provides a foundation for further development of the natural microbial consortia through the incorporation of new members, which may, in turn, further enhance waste biodegradation. The findings of this study offer insights into leveraging natural microbial communities for waste decomposition in harsh environments and understanding the ecological roles of DPANN archaea.

Conclusion

This study reveals the intricate metabolic and ecological interdependencies within a tripartite consortium of extremophilic archaea, comprising *Halorhabdus* sp. SVX81, *H. volcanii* SVX82, and *Ca*. N. occultus SVXNc. By combining transcriptomics, metabolomics, and advanced imaging techniques, the findings highlight how these organisms coordinate metabolic pathways, enabling efficient xylan degradation under hypersaline conditions. The consortium's enhanced biodegradation capabilities stem from a mutualistic exchange of metabolites, with the DPANN ectosymbiont functioning as a key metabolic partner, providing glycolytic outputs while relying on its hosts for essential biosynthetic precursors. The observed sugar accumulation in the medium suggests potential for further biotechnological optimization, including the incorporation of additional microbial partners to enhance waste decomposition. This work underscores the ecological and functional roles of DPANN archaea in microbial communities and provides a foundation for leveraging archaeal consortia in industrial applications targeting waste management in extreme environments.

Limitations of the study

The potential biotechnological significance of using archaeal consortia for xylan degradation requires confirmation through further studies employing flow cultivation approaches, as the static cultivation method used in this study demonstrated clear limitations. Consequently, statistically significant changes in xylan degradation by different consortia became evident only at the 120-h time point of cultivation. Metabolic interactions between archaeal species were predicted based on the analysis of transcriptional regulation of genes encoding key enzymes and metabolites. However, many regulated genes in these microorganisms remain unidentified or hypothetical, and those with assigned functions were predicted based on sequence homology with other known proteins. These limitations restricted the detailed analysis of metabolic interplay among consortium members.

RESOURCE AVAILABILITY

Lead contact

All requests regarding the materials generated during this project should be addressed to Michail M. Yakimov (mikhail.iakimov@cnr.it).

Materials availability

This study did not generate any new materials or reagents.

Data and code availability

- Data: Obtained whole genome sequences have been deposited at the GenBank database under the following accession numbers: *Halorhabdus* sp. SVX81 [CP104322], *H. volcanii* SVX82 [CP104741-44], and *Ca.* N. occultus SVXNc [CP104395]. Obtained RNA sequences have been deposited in NCBI as SRA records within BioProject PRJNA865582. SRA

Figure 6. Graphical summary of the pathways and systems showing differential regulation of genes in *H. volcanii* SVX82 and *Ca*. N. occultus SVXNc

The regulated genes are identified by their predicted gene names, as listed in Tables S5 and S6. The consortia in which the genes were differentially regulated are depicted using different colors for the gene names and connecting arrows, as explained in the figure legend. Genes marked as regulated exhibited at least 2-fold change in expression, with a *p* value of 0.05 or less. The following abbreviations are used in the figure: 2Oxo – 2-oxoglutarate; 2PG – 2-phospho-D-glycerate; Ac – acetate; Ac-CoA – acetyl-CoA; Arg – arginine; Asn – asparagine; Cit – citrulline; CM – chorismate; ED – Entner-Doudoroff pathway; Glu – glutamate; Gln – glutamine; Glu-p – glucose phosphate; Gly – glycine; His – histidine; Mal – malate; MTHF – 5,10-methylenetetrahydropholate; N2-ScGlu – N2-succinylglutamate; Orn – ornithine; PEP – phosphoenolpyruvate; Pro – proline; PRPP – 5-phospho-α-D-ribose 1-diphosphate; Pyr – pyruvate; Ser – serine; Suc – succinate; TCA – tricarboxylic acid cycle; THF – tetrahydropholate; Trp – tryptophan; UDP-N-Gla – UDP-N-acetyl-D-glucosamine.

accession numbers are listed in Table 1. No new software tools were designed for this study.
- Code: no program codes were generated for this project.
- All other items: no other items were generated.

ACKNOWLEDGMENTS

This study was supported by a grant from the FuturEnzyme Project (contract 101000327), funded by the European Union's Horizon 2020 Research Program and bilateral Italy-Vietnam CNR-VAST project EXPLO-Halo under grant number QTIT01.01/20-21. CryoET data were collected at the Ian Holmes Imaging Center (Bio21, University of Melbourne). D.G. is supported by an NHMRC grant (APP1196924), and a Human Frontier Science Program (HFSP) grant (RGEC33/2023). O.N.R. was supported by the National Research Foundation (NRF) of South Africa, Competitive Programme for Rated Researchers grant CPRR23030981722.

The authors thank OpenAI's DALL-E for assisting in the creation of the graphical abstract for this paper.

AUTHOR CONTRIBUTIONS

O.N.R. and M.M.Y. contributed equally to this work. Overall project design: M.M.Y., L.F.-L., M.K., and O.N.R. Project funding: M.M.Y., M.M., D.G., and O.N.R. Experimental design, culture cultivation and xylan degradation assays, DNA/RNA extraction and sequencing: V.L.C., L.M., F.C., F.S., and M.M.Y. Genome assembly, analysis, and transcriptomics: F.C. and O.N.R. Proteomics and high-performance chromatography: M.F. Cryo-ET visualization and analysis: M.M. and D.G. SEM visualization and analysis: E.A.S. and M.E.I. Biostatistics: O.N.R. Manuscript writing and editing: O.N.R., M.M.Y., M.K., M.M., D.G., L.F.-L., L.M., and F.C. Data visualization, figure design and editing: O.N.R., M.M.Y., M.M., D.G., E.A.S., and M.E.I.

DECLARATION OF INTERESTS

The authors declare no conflicts of interests.

STAR★METHODS

Detailed methods are provided in the online version of this paper and include the following:

- KEY RESOURCES TABLE
- EXPERIMENTAL MODEL AND STUDY PARTICIPANT DETAILS
- METHOD DETAILS
  - Cultivation conditions
  - Analysis of xylooligosaccharides
  - Scanning electron microscopy (SEM)
  - Cryo-electron tomography
  - DNA/RNA extraction and analysis
- QUANTIFICATION AND STATISTICAL ANALYSIS

SUPPLEMENTAL INFORMATION

Supplemental information can be found online at https://doi.org/10.1016/j.isci.2025.111749.

Received: July 24, 2024
Revised: November 7, 2024
Accepted: January 2, 2025
Published: January 4, 2025

REFERENCES

1. Madsen, E.L. (2011). Microorganisms and their roles in fundamental biogeochemical cycles. Curr. Opin. Biotechnol. *22*, 456–464.
2. Gupta, A., Sarkar, J., and Sar, P. (2019). Understanding the structure and function of extreme microbiome through genomics: Scope and challenges. In Microbial Diversity in the Genomic Era (Academic Press), pp. 581–610.
3. Ebringerova, A. (2012). The potential of xylans as biomaterial resources. In Polysaccharide Building Blocks: A Sustainable Approach to the Development of Renewable Biomaterials (Wiley), pp. 331–365.
4. Wilkie, K.C.B. (1983). Hemicellulose. Chemtech *13*, 306–319.
5. Nordahl, S.L., Preble, C.V., Kirchstetter, T.W., and Scown, C.D. (2023). Greenhouse Gas and Air Pollutant Emissions from Composting. Environ. Sci. Technol. *57*, 2235–2247.
6. Dhillon, R.S., and von Wuehlisch, G. (2013). Mitigation of global warming through renewable biomass. Biomass Bioenergy *48*, 75–89.
7. Hallsworth, J.E. (2019). Microbial unknowns at the saline limits for life. Nat. Ecol. Evol. *3*, 1503–1504. https://doi.org/10.1038/s41559-019-1021-0.
8. Li, J., Gao, Y., Dong, H., and Sheng, G.P. (2022). Haloarchaea, excellent candidates for removing pollutants from hypersaline wastewater. Trends Biotechnol. *40*, 226–239.
9. Martínez-Espinosa, R.M. (2024). Halophilic archaea as tools for bioremediation technologies. Appl. Microbiol. Biotechnol. *108*, 401.
10. Rinke, C., Schwientek, P., Sczyrba, A., Ivanova, N.N., Anderson, I.J., Cheng, J.F., Darling, A., Malfatti, S., Swan, B.K., Gies, E.A., et al. (2013). Insights into the phylogeny and coding potential of microbial dark matter. Nature *499*, 431–437.
11. Hug, L.A., Baker, B.J., Anantharaman, K., Brown, C.T., Probst, A.J., Castelle, C.J., Butterfield, C.N., Hernsdorf, A.W., Amano, Y., Ise, K., et al. (2016). A new view of the tree of life. Nat. Microbiol. *1*, 16048.
12. La Cono, V., Messina, E., Rohde, M., Arcadi, E., Ciordia, S., Crisafi, F., Denaro, R., Ferrer, M., Giuliano, L., Golyshin, P.N., et al. (2020). Symbiosis between nanohaloarchaeon and haloarchaeon is based on utilization of different polysaccharides. Proc. Natl. Acad. Sci. USA *117*, 20223–20234.
13. La Cono, V., Messina, E., Reva, O., Smedile, F., La Spada, G., Crisafi, F., Marturano, L., Miguez, N., Ferrer, M., Selivanova, E.A., et al. (2023). Nanohaloarchaea as beneficiaries of xylan degradation by haloarchaea. Microb. Biotechnol. *16*, 1803–1822.
14. Reva, O., Messina, E., La Cono, V., Crisafi, F., Smedile, F., La Spada, G., Marturano, L., Selivanova, E.A., Rohde, M., Krupovic, M., and Yakimov, M.M. (2023). Functional diversity of nanohaloarchaea within xylan-degrading consortia. Front. Microbiol. *14*, 1182464.
15. Dombrowski, N., Lee, J.H., Williams, T.A., Offre, P., and Spang, A. (2019). Genomic diversity, lifestyles and evolutionary origins of DPANN archaea. FEMS Microbiol. Lett. *366*, fnz008.
16. Zhang, I.H., Borer, B., Zhao, R., Wilbert, S., Newman, D.K., and Babbin, A.R. (2024). Uncultivated DPANN archaea are ubiquitous inhabitants of global oxygen-deficient zones with diverse metabolic potential. mBio *15*, e0291823.
17. Quadri, S.R., Jin, P., Wang, K., Qiao, H., Dhulappa, A., Luo, Z.H., Wang, S., and Narsing Rao, M.P. (2024). Taxonomic Reframe of Some Species of the Genera *Haloferax* and *Halobellus*. Curr. Microbiol. *81*, 216.
18. Petibon, C., Malik Ghulam, M., Catala, M., and Abou Elela, S. (2021). Regulation of ribosomal protein genes: An ordered anarchy. Wiley Interdiscip. Rev. RNA *12*, e1632.
19. West-Roberts, J.A., Valentin Alvarado, L.E., Mullen, S., Sachdeva, R., Smith, J., Hug, L.A., Gregoire, D., Liu, W., Lin, T.Y., Husain, G., and Amano, Y. (2023). Giant genes are rare but implicated in cell wall degradation by predatory bacteria. Preprint at bioRxiv. https://doi.org/10.1101/2023.11.21.568195v1.full.pdf.
20. Hamm, J.N., Liao, Y., von Kügelgen, A., Dombrowski, N., Landers, E., Brownlee, C., Johansson, E.M.V., Whan, R.M., Baker, M.A.B., Baum, B., et al. (2024). The parasitic lifestyle of an archaeal symbiont. Nat. Commun. *15*, 6449.
21. Reva, O.N., La Cono, V., Crisafi, F., Smedile, F., Mudaliyar, M., Ghosal, D., Giuliano, L., Krupovic, M., and Yakimov, M.M. (2024). Interplay of

intracellular and trans-cellular DNA methylation in natural archaeal consortia. Environ. Microbiol. Rep. *16*, e13258.

22. Rodrigues-Oliveira, T., Souza, A.A., Kruger, R., Schuster, B., Maria de Freitas, S., and Kyaw, C.M. (2019). Environmental factors influence the *Haloferax volcanii* S-layer protein structure. PLoS One *14*, e0216863.
23. Alvarez, M., Schrey, A.W., and Richards, C.L. (2015). Ten years of transcriptomics in wild populations: what have we learned about their ecology and evolution? Mol. Ecol. *24*, 710–725.
24. Hackley, R.K., and Schmid, A.K. (2019). Global Transcriptional Programs in Archaea Share Features with the Eukaryotic Environmental Stress Response. J. Mol. Biol. *431*, 4147–4166.
25. Comolli, L.R., Baker, B.J., Downing, K.H., Siegerist, C.E., and Banfield, J.F. (2009). Three-dimensional analysis of the structure and ecology of a novel, ultra-small archaeon. ISME J. *3*, 159–167.
26. Klingl, A. (2014). S-layer and cytoplasmic membrane - exceptions from the typical archaeal cell wall with a focus on double membranes. Front. Microbiol. *5*, 624.
27. Sutter, J.M., Johnsen, U., Reinhardt, A., and Schönheit, P. (2020). Pentose degradation in archaea: *Halorhabdus* species degrade D-xylose, L-arabinose and D-ribose via bacterial-type pathways. Extremophiles *24*, 759–772.
28. Kuprat, T., Johnsen, U., Ortjohann, M., and Schönheit, P. (2020). Acetate Metabolism in Archaea: Characterization of an Acetate Transporter and of Enzymes Involved in Acetate Activation and Gluconeogenesis in *Haloferax volcanii*. Front. Microbiol. *11*, 604926.
29. Widdel, F., Kohring, G.W., and Mayer, F. (1983). Studies on dissimilatory sulfate-reducing bacteria that decompose fatty-acids III. Characterization of the Filamentous Gliding *Desulfonema limicola* gen. nov sp. nov., and *Desulfonema magnum* sp. nov. Arch. Microbiol. *134*, 286–294.
30. Pfennig, N., and Lippert, K.D. (1966). Über das vitamin B12-bedürfnis phototropher Schwefelbakterien. Arch. Mikrobiol. *55*, 245–256.
31. Borges, T.A., Souza, A.T.d., Squina, F.M., Riaño-Pachón, D.M., Santos, R.A.C.d., Machado, E., Oliveira, J.V.d.C., Damásio, A.R., and Goldman, G.H. (2014). Biochemical characterization of an endoxylanase from *Pseudozyma brasiliensis* sp. nov. strain GHG001 isolated from the intestinal tract of *Chrysomelidae* larvae associated to sugarcane roots. Process Biochem. *49*, 77–83.
32. Kremer, J.R., Mastronarde, D.N., and McIntosh, J.R. (1996). Computer visualization of threedimensional image data using IMOD. J. Struct. Biol. *116*, 71–76.
33. Agulleiro, J.I., and Fernandez, J.J. (2011). Fast tomographic reconstruction on multicore computers. Bioinformatics *27*, 582–583.
34. Wei, S., Cui, H., Zhang, Y., Su, X., Dong, H., Chen, F., and Zhu, Y. (2019). Comparative evaluation of three archaeal primer pairs for exploring archaeal communities in deep-sea sediments and permafrost soils. Extremophiles *23*, 747–757.
35. Contreras-Moreira, B., and Vinuesa, P. (2013). GET_HOMOLOGUES, a versatile software package for scalable and robust microbial pangenome analysis. Appl. Environ. Microbiol. *79*, 7696–7701.
36. Hammer, Ø., Harper, D.A., and Ryan, P.D. (2001). PAST: Paleontological statistics software package for education and data analysis. Palaeontol. Electron. *4*, 9.
37. Anderson, M.J. (2008). A new method for non-parametric multivariate analysis of variance. Austral Ecol. *26*, 32–46.

STAR★METHODS

KEY RESOURCES TABLE

REAGENT or RESOURCE	SOURCE	IDENTIFIER
Bacterial and virus strains		
Haloferax volcanii SVX82 (former *Haloferax lucertense* SVX82)	Russia: Razval and Ozero Dunino lakes, Sol-Iletsk region	SAMN30630946
Ca. Nanohalococcus occultus SVXNc	Russia: Razval and Ozero Dunino lakes, Sol-Iletsk region	SAMN30630938
Halorhabdus sp. SVX81	Russia: Razval and Ozero Dunino lakes, Sol-Iletsk region	SAMN30630960
Deposited data		
H. volcanii SVX82 (whole genome sequence)	GenBank	CP104741-44
Ca. N. occultus SVXNc (whole genome sequence)	GenBank	CP104395
Halorhabdus sp. SVX81 whole genome sequence)	GenBank	CP104322
RNA sequences from consortium I (*H. volcanii* SVX82)	SRA	SRX22141247 SRX22141248
RNA sequences from consortium II (*H. volcanii* SVX82 + *Ca*. N. occultus SVXNc)	SRA	SRX22141249 SRX22141236
RNA sequences from consortium III (*Halorhabdus* sp. SVX81 + *H. volcanii* SVX82)	SRA	SRX22141237 SRX22141238
RNA sequences from consortium IV (*Halorhabdus* sp. SVX81 + *H. volcanii* SVX82 + *Ca*. N. occultus SVXNc)	SRA	SRX22141239 SRX22141240 SRX22141241

EXPERIMENTAL MODEL AND STUDY PARTICIPANT DETAILS

The model microorganisms used in this study were halophilic archaea isolated from a natural xylan-degrading consortium,[12–17,21] consisting of the xylan-degrading *Halorhabdus* sp. SVX81, the xylose-consuming *H. volcanii* SVX82 and its ectosymbiont *Ca*. N. occultus SVXNc, were analyzed in various compositions.

This study did not include any animals, human participants, cell lines or any other methods, which would require special permissions or ethical approvals by the research institutes.

METHOD DETAILS

Cultivation conditions

Four experimental groups were created to elucidate possible interactions among the consortium members, cultivated either on D-xylose, or beech wood xylan as the sole carbon source (Table 1). All experimental settings used previously described LC liquid mineral medium.[12] After sterilization (121°C, 20 min) and cooling, the pH was adjusted to 7.2 by the adding sterile 1M KOH. The medium was additionally supplemented with 1 mL L^{-1} of the 1,000 × trace element SL-10 solution prepared as describe elsewhere[29] and including 50 mg L^{-1} yeast extract and 1 mL L^{-1} of vitamin mix[30] containing 5.0 mg L^{-1} thiamine (vitamin B1), 5.0 mg L^{-1} calcium pantothenate, 2.0 mg L^{-1} biotin, 5.0 mg L^{-1} p-aminobenzoic acid (PABA), 5.0 mg L^{-1} nicotinic acid (niacin), 10.0 mg L^{-1} pyridoxine (vitamin B6), 2.0 mg L^{-1} folic acid, 5.0 mg L^{-1} riboflavin (vitamin B2), and 0.5 mg L^{-1} cobalamin (vitamin B12). Vitamins were obtained from Merck Life Science S.r.l. (Milan, Italy), dissolved separately, sterilized through 0.22 μm nylon filters (Sigma-Aldrich, product number WHA99102502), and then combined into a stock solution.

Sterilized beech wood xylan (Megazyme, catalogue number P-XYLNBE-10G) was added at a final concentration of 2.0 g L^{-1} to the growth broth for cultivation of xylan-degrading archaeal consortia. For cultivation of xylose-consuming consortia, which are unable to degrade xylan,[12] 10 mM D-xylose was added instead of the beech wood xylan. All cultures were incubated in 120 mL serum vials (in triplicate) in a thermostat at 40°C, statically, to create microaerobic conditions. Their growth was observed over a 240 h period. The same cultures were used for all downstream analyses including transcriptomics, scanning electron microscopy (SEM) and electron cryotomography (cryo-ET).

The initial xylan content in the control (abiotic) experiment and in the experimental groups was within the range of 1,890 ± 60 (standard deviation – SD) mg L^{-1}, corresponding to 94.5 ± 3.0% of the added amount of xylan (2,000 mg L^{-1}), thus confirming the reliability of the chosen xylan precipitation method for its detection in solutions. The variation in xylan content in the abiotic group over time was measured after 72 h of incubation and at the end of the experiment (240 h), ranging between 1,840 ± 80 mg L^{-1} and 1,800 ± 50 mg L^{-1}, respectively, indicating the stability of added polysaccharide at high salinity and 40°C throughout the experiment.

Xylan consumption by both the SVX81 axenic culture and the consortia containing *Halorhabdus* sp. SVX81 was monitored throughout the experiment using a modified precipitation method of the Azo-Xylan (Megazyme, catalogue number S-AXBL).[31] Briefly, 15 mL from each xylan-supplemented experiment was collected after 72, 120 and 240 h of cultivation and clarified by centrifugation at 9,000 × g for 15 min at 4°C. The biomass pellet and supernatant were separated, and xylan was further precipitated by adding 25 mL of precipitation solution (40 g L^{-1} $CH_3COONa \cdot 3H_2O$ and 4.0 g L^{-1} $Zn(CH_3COO)_2 \cdot 2H_2O$ in 77% (v/v) ethanol in MilliQ water, pH 5.0) to 10 mL of supernatant and leaving the reaction mixture at room temperature for 1 hour. The precipitated xylan was then collected by centrifugation at 2,000 × g for 10 min at 4°C and the resulting pellet was left to dry completely in an oven at 65°C for 24 hours. The dry weight of residual beech wood xylan was then measured and the rate of its degradation during the experiments was calculated as difference between the amounts of xylan harvested from parallel abiotic controls. Experiments were conducted in triplicate, and mean values with standard deviations were calculated using the NumPy v.1.26.4 library in Python 3. Statistical significance of differences in xylan concentration across the culture media of different consortia was assessed by calculating *p*-values from independent two-sample t-tests using the stats.ttest_ind function from the scipy v.1.11.2 library in Python 3. The library matplotlib v.3.8.3 was used in Python 3 for result visualisation.

Analysis of xylooligosaccharides

Xylooligosaccharides were analyzed by high-performance anion-exchange chromatography with pulsed amperometric detection (HPAEC-PAD), following a slightly modified approach that we described previously.[13] Briefly, the supernatant of triplicates (each aliquot of 300 μl), obtained by centrifuging the corresponding growing culture at 9000 × g for 15 min at 4°C, was pooled together and absolute ethanol was added to a final ethanol concentration of 80% (v/v) and then centrifuged at 10,000×g for 10 min at 4°C to precipitate both extracellular proteins and exopolysaccharides, including remaining high molecular weight xylan. Replica pooling was done specifically to reduce the total number of samples to avoid extensive "ion poisoning" of the column due to the high salinity of the samples, which significantly reduces the sensitivity of the analysis. Supernatants (250 μL aliquots) were than diluted 10-times with MilliQ water and filtered through 0.22 μm nylon filters (Sigma-Aldrich, product number WHA99102502). Xylooligosaccharide analysis was performed using an HPAEC-PAD, Dionex ICS3000 system, CarboPack PA-100 anion-exchange column (4 mm × 250 mm) coupled to a CarboPac PA-100 guard column (4 m × 50 mm), and an autosampler (model AS-HV), as described elsewhere.[13] Identification of xylooligosaccharides containing up to six units (xylose, xylobiose, xylotriose, xylotetrose, xylopentose and xylohexose) was carried out by comparing the retention times of the corresponding standards (all provided by Megazyme, NEOGEN Europe Ltd).

Scanning electron microscopy (SEM)

Cells grown in LC liquid mineral medium supplemented with xylan (2 g L^{-1}) were fixed with 2.5% glutaraldehyde (v/v, final concentration) for 1 hour. The fixative was removed by washing twice with LC mineral medium. The fixed material was placed onto poly-L-lysine-coated coverslips for 10 min to cross-link microbes with poly-L-lysine coating. Dehydrating was achieved using a series of increasing of acetone in water mixtures (10, 30, 50, 70, 90% (v/v) acetone) and pure acetone on ice for 10 min for each step. Once in 100% acetone, samples were allowed to reach room temperature while being replenished with fresh 100% acetone. The samples were then subjected to critical-point drying with liquid CO_2 (Quorum K850 Critical Point Dryer, Quorum Technologies Ltd., London, UK). The dried samples were covered with a gold film by sputter coating (Quorum Q150R S plus; Quorum Technologies Ltd., London, UK) before examination in a scanning electron microscope TESCAN Mira 3 (Tescan Brno s.r.o., Brno, Czech Republic) with an acceleration voltage of 5 kV. The haloarchaeal members of the tripartite consortium were easily distinguishable by cell morphology. Whereas *Halorhabdus* sp. SVX81 cells under all experimental conditions presented a rod-shaped morphology, *H. volcanii* SVX82 cells were pleomorphic, with the majority of cells (~75%) existing as erythrocyte-like flat disks, consistent with previous observations.[13]

Cryo-electron tomography

The cryo-electron tomography (Cryo-ET) procedures were explained in detail in the previous publications.[21,32,33] Samples for the cryo-ET analysis were prepared from the *H. volcanii* SVX82 and *Ca*. N. occultus SVXNc (*Hv+No*) bipartite consortium grown on xylose, and the tripartite consortium including *Halorhabdus* sp. SVX81, *H. volcanii* SVX82 and *Ca*. N. occultus SVXNc grown on xylan.

DNA/RNA extraction and analysis

All these procedures were described in detail in the previous publication.[21]

RNA was extracted from 5 mL of triplicate cultures at the late exponential phase using the MasterPure™ Complete DNA and RNA Purification Kit (Epicentre, VWR, Milan, Italy). Cells were harvested by centrifugation at 10,000 × g, 4°C, for 20 min, and RNA extraction followed the manufacturer's instructions. The RNA was resuspended in 50 μL of RNase-free water and treated with the TURBO

DNA-free kit (Ambion, TX, USA) to remove residual DNA. RNA quality and concentration were measured using the Qubit 3.0 fluorometer (Thermo Fisher Scientific, Italy). DNA removal was confirmed by PCR amplification with Arch519F/Arch915R primers,[34] targeting Halobacteria. PCR was performed on a MasterCycler 5331 Gradient PCR (Eppendorf, Hamburg, Germany) with the following conditions: 94°C for 5 min; 35 cycles of 94°C for 1 min, 50°C for 1 min, and 72°C for 2 min; followed by 72°C for 10 min. No PCR products were detected on a 1% agarose gel. RNA integrity was assessed using the Agilent 2100 Bioanalyzer (Agilent Technologies). After rRNA depletion and DNase treatment, sequencing was performed by FISABIO (Valencia, Spain) using the Illumina® NextSeq platform with 2 × 100 bp paired-end libraries (NextSeq Reagent Kit v2.5). Metatranscriptome analysis and quality checks were conducted with PRINSEQ-lite.

QUANTIFICATION AND STATISTICAL ANALYSIS

Transcriptional analysis was conducted using Bioconductor version 3.17 on R-3.4.4. RNA sequences were aligned against the reference genomes of the respective organisms available at the Genbank database. The featureCounts in Bioconductor's Rsubread v.2.0.1 package counted reads over coding sequences (CDS). DESeq2 v.1.26.0 and GenomicFeatures v.1.38.2 normalized counts by total reads and CDS lengths, analyzing gene expression, fold changes, and *p*-values across datasets. Gene regulation involving an absolute expression fold change of 2 or greater, with a *p*-value of 0.05 or less, was considered statistically significant.

Pairs of homologous genes shared by *Halorhabdus* sp. SVX81 and *H. volcanii* SVX82 were identified using the GET_HOMOLOGUES v.2602020 program with default parameters.[35] Fold change values of gene expression predicted by the program DESeq2 were used to calculate Pearson product-moment correlation of gene regulation using function stats.pearson of the library scipy v.1.11.2 in Python 3. The two-tailed *p*-value of Pearson correlation was calculated using function stats.t.cdf of the same library. Principal Component Analysis (PCA) algorithm, implemented in the PAleontological STatistics (PAST) 4.02 program (http://folk.uio.no/ohammer/past/),[36] was used for clustering gene expression patterns of *H. volcanii* SVX82 in different consortia. For the PCA analysis, reads per kilo base per million mapped reads (RPKM) values of gene expression were calculated by Equation 1:

$$RPKM_g = \frac{10^9 \times N_{mapped\_reads\_per\_gene}}{Total\_mapped\_reads \times gene\_length} \quad \text{(Equation 1)}$$

Before PCA clustering, row-scaling normalization of RPKM values for the same genes, determined under different growth conditions, was performed by dividing all values in each row by the highest RPKM value in that row (Table S1). Row-scaling normalization is necessary to eliminate the dominance of highly expressed genes during PCA analysis. The program PAST was used to draw estimated 95% confidence ellipses for the distribution of gene expression patterns on the PCA plot. Statistical significance of differences between gene expression patterns was calculated using the Permutational Multivariate Analysis of Variance (PERMANOVA) algorithm,[37] implemented as the stats.distance function in the skbio v.0.6.2 library in Python 3 using the default settings of arguments (999 permutations).

Additional information regarding the numbers of experiments and definitions of deviation bars can be found in the section results and in figure legends.